Surface and Barrier Properties of Hybrid Nanocomposites Containing Silica and PEO Segments

Giulio Malucelli,[1] Aldo Priola,[1] Ezio Amerio,[1] Antonino Pollicino,[2] Giovanna di Pasquale,[2] Diego Pizzi,[3] Maria Grazia de Angelis,[3] Ferruccio Doghieri[3]

[1]*Politecnico di Torino, Dipartimento di Scienza dei Materiali ed Ingegneria Chimica and Local INSTM Unit, C.so Duca degli Abruzzi 24, 10129 Torino, Italy*
[2]*Università di Catania, Dipartimento Metodologie Fisiche e Chimiche per l'Ingegneria and Local INSTM Unit, V.le A. Doria 6, 95125 Catania, Italy*
[3]*Università di Bologna, Dipartimento di Ingegneria Chimica, Mineraria e delle Tecnologie Ambientali and Local INSTM Unit, Via Terracini 34, 40131 Bologna, Italy*

Received 16 May 2006; accepted 28 September 2006
DOI 10.1002/app.25562
Published online in Wiley InterScience (www.interscience.wiley.com).

ABSTRACT: Hybrid organic–inorganic nanocomposites containing PEO segments linked to a methacrylate network were prepared through a dual-curing process, which involved photopolymerization and condensation of alkoxysilane groups. A system based on an α,ω-dimethacrylate PEO oligomer (BEMA 1400) added with methacryloyl-oxypropyl-trimethoxysilane (MEMO) and tetraethoxysilane (TEOS) was used. The surface properties of the obtained films were investigated through XPS analyses and contact angle measurements. A selective enrichment of the MEMO additive towards the outermost layers of the films was evidenced either in the presence or in the absence of TEOS. SEM analyses were performed on the cross section of the films coated on PET substrates, determining the film composition at different depth by EDS analysis. The Si content was found constant, moving from the PET surface towards the air–surface of the films. The barrier properties, with respect to oxygen, of the hybrid films coated on a PET substrate were measured. A decrease of the permeability and of the oxygen transmission rate using hybrid coatings was observed. © 2006 Wiley Periodicals, Inc. J Appl Polym Sci 103: 4107–4115, 2007

Key words: hybrid silica nanocomposites; dual-curing; surface properties; barrier properties

INTRODUCTION

In the last few years the so-called hybrid materials or ceramers have risen a great interest as new materials because of their peculiar properties. They are characterized by a biphasic morphology where an organic phase is strictly interconnected with an inorganic one at a nanometric level. These materials provide to combine the high ductility and low temperature processing conditions of polymers with the outstanding properties of ceramics, such as high modulus and mechanical properties, thermal stability, and low coefficient of thermal expansion.[1–6] Recently, they have been proposed for packaging applications.[7]

Several hybrids based on SiO_2, TiO_2, ZrO_2, $CaCO_3$ have been proposed and investigated in the presence of different polymeric matrices.[8–11] The preferred way for the synthesis of the inorganic phase is based on the sol–gel process, which involves a two-step hydrolysis and condensation reaction, usually starting from metal alkoxides or functionalized metal alkoxides.

Recently, we proposed the preparation of hybrid organic–inorganic materials through a dual curing process involving an UV curing reaction followed by a thermal condensation of metal alkoxide groups.[12] This process combines the advantages connected to the UV-curing technique, such as a rapid and solvent-free polymerization, with the sol–gel process flexibility. In this context, we have used as organic precursor a PEO oligomer which ends by α,ω methacrylic groups. The oligomer was added with methacryloyl-oxypropyl-trimethoxysilane (MEMO) as linking agent of organic and inorganic phases and with tetraethoxysilane (TEOS) as inorganic precursor.

A similar technique was used by Cho et al.[13] and by Zou and Soucek,[14] who described the preparation of hybrid coatings having improved properties, such as scratch-resistance, abrasion, heat, and radiation resistance, together with improved mechanical, electrical, and optical properties.

In this work, we investigated the surface properties of the hybrid systems by means of XPS analysis and contact angle measurements; moreover, the silicon distribution in the bulk was examined by SEM microscopy. The obtained data were correlated to the permeability of the hybrid films coated on a PET sub-

Correspondence to: G. Malucelli (giulio.malucelli@polito.it).
Contract grant sponsor: MIUR; contract grant number: PRIN 2004, Prot. 2004030304.
Contract grant sponsor: Regional Funds; contract grant number: Progetto Piemonte RSA 2004, D26.

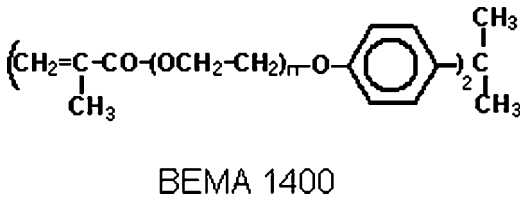

Figure 1 Structure of BEMA 1400 oligomer.

strate towards oxygen, to check their barrier properties and their interest in packaging applications.[7]

EXPERIMENTAL

Materials

PEO oligomer is a bisphenol-A polyethoxylate (15 EO/phenol) dimethacrylate (BEMA 1400, from Aldrich). The structure of BEMA 1400 is shown in Figure 1; n is $\sim$ 15. Methacryloyl-oxypropyl-trimethoxysilane (MEMO), tetramethoxysilane (TMOS), tetraethoxysilane (TEOS), hydrochloric acid, and dibuthyltin diacetate (condensation catalyst) are Aldrich products and are used as received.

In the text the following names are used to indicate the different mixtures:

BEMA 1400: pure methacrylate oligomer.
BEMA: mixture of BEMA 1400 oligomer with 20% (w/w) MEMO.

As photoinitiator, 2-hydroxy-2-methyl-1-phenyl propan-1-one (Darocur 1173 from Ciba Specialty Chemicals) was employed.

PET films (3M products, thickness = 36 μm, crystallinity = 36.5%) were used as a substrate.

Preparation of the hybrid films

A typical UV-curable mixture was prepared by adding MEMO (20% w/w) to BEMA 1400 oligomer. Then TEOS was added in different amounts, up to 70% (w/w). The obtained mixture was added with 4% of Darocur 1173 as photoinitiator, of water (alkoxy/water molar ratio = 2), and of 2% of both dibutyltin diacetate and HCl conc. solution. The adopted procedure is reported elsewhere.[12] The mixture was coated on a PET substrate by using a wire wound applicator (thickness of the coating, 1.2 ± 0.1 μm) and subjected to the dual-curing process. The photochemical curing was performed by using a medium vapor pressure Hg UV lamp (Helios Italquartz, Italy), with radiation intensity on the surface of the sample of 20 mW/cm^2, working in N_2 atmosphere.[15] After the UV-curing, the condensation reaction was performed by treating the photocured films at 75°C for 4 h, to obtain the completion of the condensation process. The sequence of the reactions involved in the adopted dual-curing process is shown in Figure 2; all the procedure is reported elsewhere.[12]

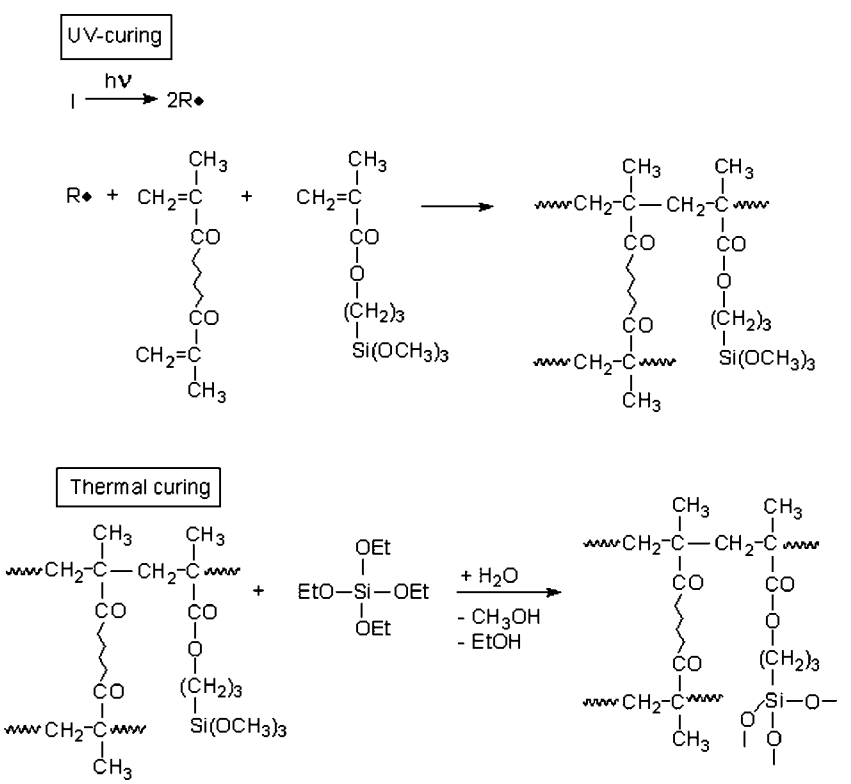

Figure 2 Scheme of the sequence of the reactions involved in the dual-curing process.

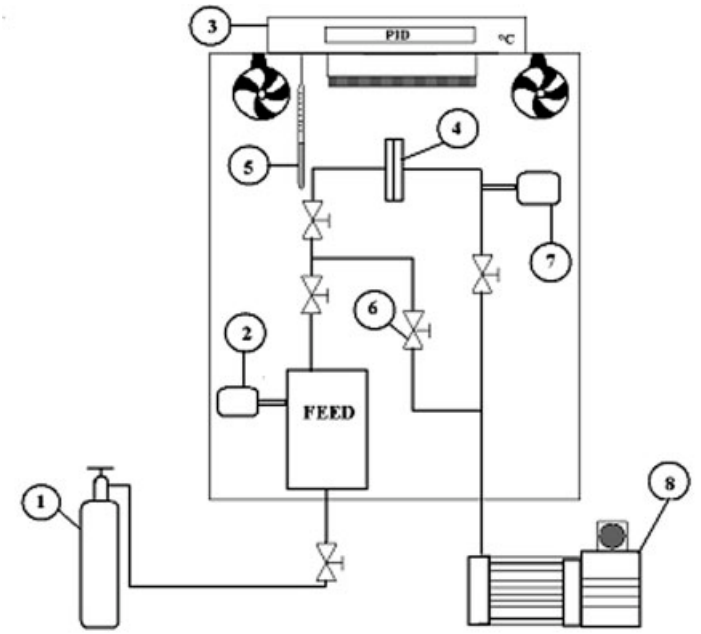

1: Oxygen reservoir
2: High-pressure manometer (FS 10 bar)
3: Thermo regulator
4: Sample cell
5: Thermocouple
6: Bypass valve
7: Low-pressure manometer (FS 10 mbar)
8: Vacuum pump

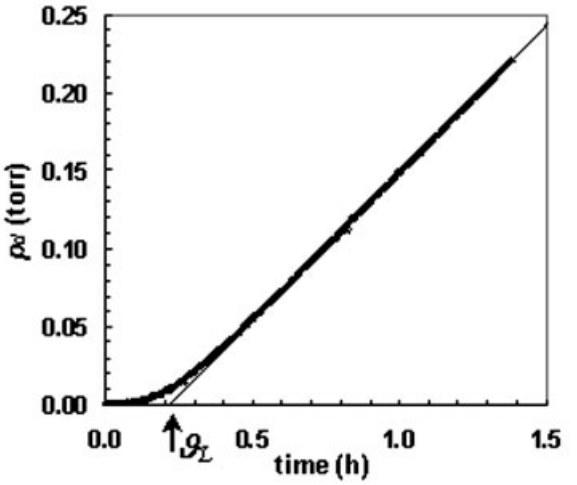

Output of the permeation experiment and time-lag θ_L determination (p_d= pressure measured by the low-pressure manometer (7))

Figure 3 Scheme of the experimental apparatus for evaluating the transport properties.

Analysis and characterization

Contact angle measurements were performed with a Kruss DSA10 instrument, equipped with a video camera; analyses were made at room temperature by means of the sessile drop technique. Three to five measurements were performed on every sample and the values averaged. The measuring liquid was *n*-hexadecane.

XPS measurements were carried out on a VG Instrument electron spectrometer using a Mg $K_{\alpha,1,2}$ X-ray source (1253.6 eV). The X-ray source in the standard conditions had been working at 100 W, 10 kV, and 10 mA. The base pressure of the instrument was 5×10^{-10} Torr and an operating pressure of 2×10^{-8} Torr was adopted. A pass energy of 100, 50, and 20 eV was used for widescans, narrowscans, and curve fitting, respectively. The semiquantitative surface analyses were carried out by the determination of the photoelectron peak areas obtained by multiplying the experimental values with the appropriate sensitivity factor. Three different take off angles (t.o.a.: 25, 45, and 80°) were used to get some information concerning the depth profiles: considering that the relationship between the depth of the analyzed layer (d) and the t.o.a. (θ) is represented by the equation $d = 3\lambda \sin \theta$, where λ is the average free path of the photoelectrons (for carbon $\lambda = 14$ Å), it is possible to quantify the thickness of the film analyzed at the three different t.o.a., which corresponds to about 20, 30, and 40 Å, respectively. The calculation of the areas corresponding to the different photoelectron peaks was performed using VGX900x software; the curve fitting elaborations were done by means of PeakFit software (version 4, from SPSS Inc.). Binding energy were referred to the C—H level at 285 eV.

The film thickness was measured by means of a Coating Thickness Gauge Quanix 7500 from DR.NIX GmbH Koln (Germany).

SEM analyses were performed on the cross-section of the films (thickness = 10 μm), coated on PET substrates, by using a JEOL mod. JSM6400 apparatus. The film composition at different depth was determined by EDS analysis (EDS Oxford mod. 6506).

The adhesion of the coatings on PET films was checked by crosshatching technique (DIN 5315), making the crosscut incision with a ten-blade cutter, followed by tape treatment (tape adhesion).

TABLE I
Properties of the Cured Systems

Type of coating	T_g DSC (°C)	T_g DMTA (°C)	Gel content (%)	SiO_2 content[a] (%)
BEMA	−32.0	−23.2	98	0
BEMA + 30% w/w TEOS	−18.0	−5.6	98	11
BEMA + 50% w/w TEOS	−8.0	14.0	99	22
BEMA + 70% w/w TEOS	−1.2	16.1	99	40

[a] Based on TEOS content.

The evaluation of the barrier properties of the coatings with respect to pure Oxygen (SIAD product, Italy; purity = 99.5%) was performed using the experimental apparatus schematized in Figure 3, together with the typical graphical output of the experiment. The apparatus is a closed-volume manometric device previously described.[16] The film is placed in a stainless steel cell, leakage-proof tightened to maintain vacuum in the downstream side, while the upstream side is put in contact with a vessel containing the pure oxygen at high pressure; the whole apparatus is placed in an air-thermostated environment. The pressure in the downstream vessel, p_d, increases with time because of gas permeation through the sample and is recorded by the low-pressure manometer (No. 7 in Fig. 3). At steady state, the amount of gas moles passed in the unit time interval is constant, i.e., the pressure p_d increases linearly with time. The permeability P is defined as:

$$P \overset{\text{DEF}}{\equiv} \frac{J_{ST} l}{\Delta p} = \left(\frac{dp_d}{dt}\right)_{t\to\infty} \frac{V}{RTA} \frac{l}{\Delta p} \tag{1}$$

where Δp is the pressure difference across the film, l the film thickness, J_{ST} the steady state gas flux, i.e., the number of gas moles passed per unit time and unit surface area of the film, at the steady state. As it is expressed in the second part of eq. (1), J_{ST} can be calculated, based on the ideal gas law, from the value of the downstream volume V, the temperature T, the area A of the film, and the slope of the straight line representing the p_d versus t plot in the steady state ($t \to \infty$). In the apparatus, V is equal to 24 cm^3 and the film area A is equal to 9.6 cm^2, while the Δp is maintained at 2 or 4 bar during experiments.

The intercept on the t axis of p_d versus t plot in the steady state is called time-lag (ϑ_l) and it measures the characteristic time of the permeation process. If p_d is negligible compared to the upstream pressure and the film is initially gas-free, the time-lag value is related to the diffusivity, D, of the gas in the material, through the following equation:

$$\vartheta_l = \frac{l^2}{6D} \tag{2}$$

For homogeneous films, the permeability and diffusivity calculated using eqs. (1) and (2) are physicochemical properties, that depend only on temperature and on the gas and polymer nature, while for multilayer samples they are apparent quantities, depending on the geometry of the sample. A useful operative information is given by the gas permeance through the film, or transfer rate (TR), defined as follows:

$$\text{TR} \overset{\text{DEF}}{\equiv} \frac{J_{ST}}{\Delta p} = \frac{P}{l} \tag{3}$$

The permeance is referred to the specific sample, depending upon the film thickness.

The permeability of the hybrid coating, P_c, can be evaluated from the permeance of the coated polymer, $(TR)_{cp}$, and the permeability of the pure substrate, P_p, and the polymer and coating thickness values, l_c and l_p:

$$\frac{1}{(TR)_{cp}} = \frac{l_p}{P_p} + \frac{l_c}{P_c} \tag{4}$$

To measure the oxygen transfer rate (OTR) and, as far as the kinetics of the process is concerned, the time-lag data, two different temperatures (35 and 65°C) were chosen. Moreover, the values of permeability and diffusivity of oxygen in pure PET and in the hybrid layer were evaluated.

RESULTS AND DISCUSSION

Bulk properties of the cured systems

In Table I some properties of the cured systems used in this work are collected. The hybrid films containing TEOS show an increase of T_g values: it can be attributed to the decrease of mobility of PEO segments in the presence of silica as reported previously.[12,17]

XPS analyses

First of all films of BEMA1400/MEMO (80/20 w/w, without TEOS) were considered. In Figure 4(A), a typical widescan spectrum recorded at t.o.a. = 25° is reported. The spectrum shows the presence of C (≈ 285 eV), O (≈ 532 eV), and Si (≈ 102 eV).

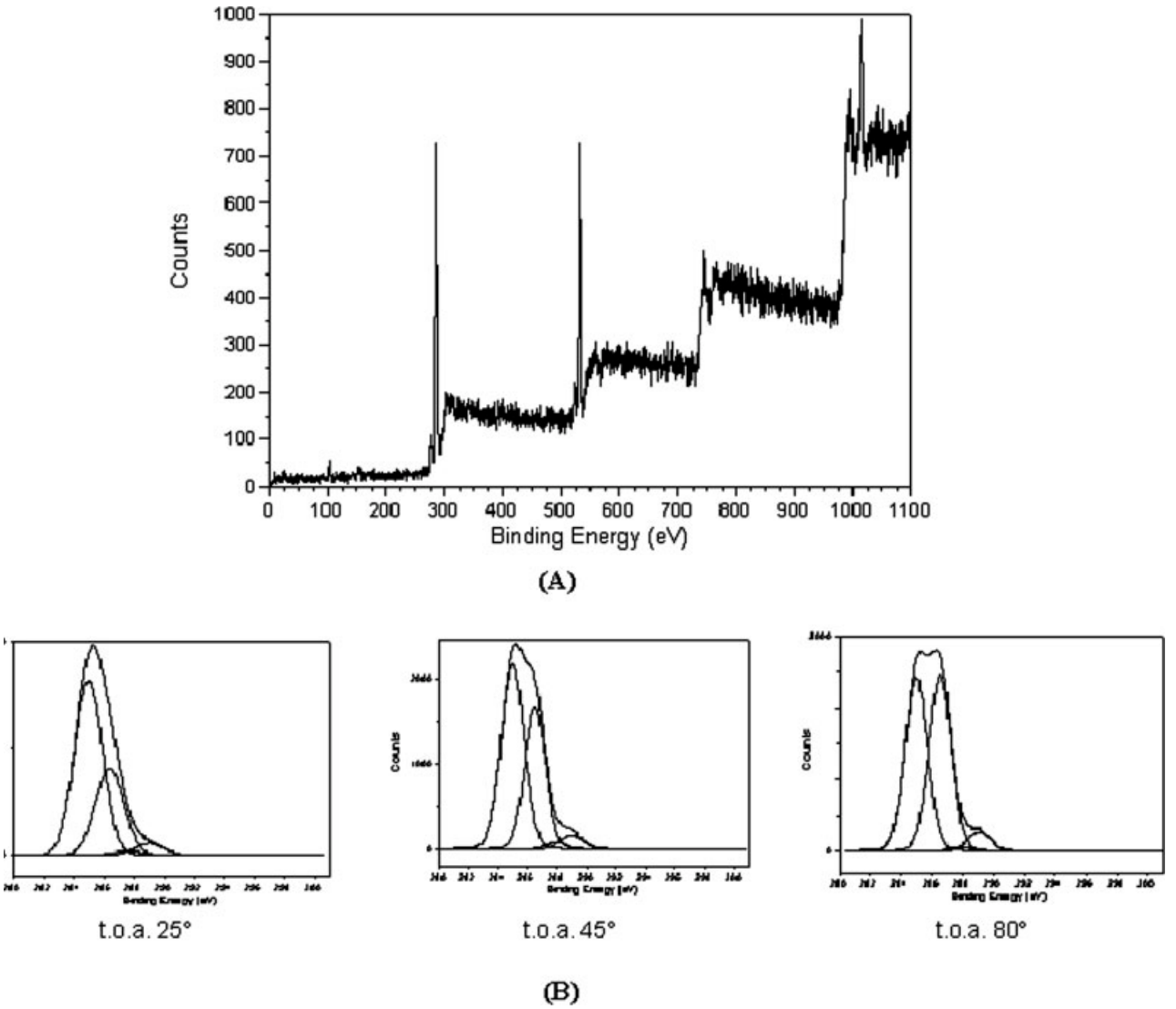

Figure 4 (A) XPS widescan spectrum at t.o.a. = 25° for BEMA/MEMO (80/20) film; (B) curve fitting of C_{1s} envelope at different toa for BEMA/MEMO (80/20) film.

In Table II the atomic ratios, which were calculated from the areas of the photoelectron peaks, are collected, together with the theoretical values determined on the basis of the composition of the mixture. The Si/O atomic ratio on the very surface of the films is higher (more than three times) than that expected on the basis of the bulk composition. The Si/O ratio decreases by increasing the t.o.a., i.e., by increasing the depth of surface analyzed. On the other hand, the C/O ratio slightly increases by increasing the t.o.a.

It is important to note that the experimental C/O ratio is influenced, as frequently observed in studying polymer surfaces by XPS, by a variable amount of hydrocarbon contamination[18]; for this reason it is not

TABLE II
Experimental Atomic Ratios, Calculated Hydrocarbon Contamination, and Corrected Atomic Ratios at Different t.o.a. for BEMA UV-Cured Films

Take-off angle (°)	Experimental C/O	Experimental Si/O	Calculated hydrocarbon contamination (%)	Corrected C/O
25	3.57	0.13	55	2.30
45	3.12	0.10	28	2.44
80	2.78	0.11	11	2.50
Theoretical composition	*2.50*	*0.04*	*0*	*2.50*

TABLE III
Experimental Atomic Ratios and Corrected From Hydrocarbon Contamination Atomic C/O Ratio at Different t.o.a. for BEMA + 70% TEOS Hybrid Films

Take-off angle (°)	Experimental C/O	Experimental Si/O	Calculated hydrocarbon contamination (%)	Corrected C/O
25	2.72	0.39	125	1.09
45	1.90	0.37	68	1.14
80	1.60	0.35	33	1.21
Theoretical composition	*1.25*	*0.27*	*0*	*1.25*

possible to get straight information from it. To evaluate the hydrocarbon contamination and to determine a semiquantitative composition of the outermost layers, the curve fitting of C_{1s} envelope was studied at different take off angles.

On the basis of the feeding, the percentage abundance of the four components, which form the whole C_{1s} envelope (a component centered at 285.0 eV due to carbon atoms not bonded to oxygen (C—H, or C—C); a component centered at about 286.5 eV arising from carbon atoms single bonded to oxygen; a component centered at about 288 eV arising from carbon atoms double bonded to oxygen, and a component centered at about 289 eV arising from carboxylic functions), would have been 35%, 60.5%, 0.5%, and 4%, respectively.

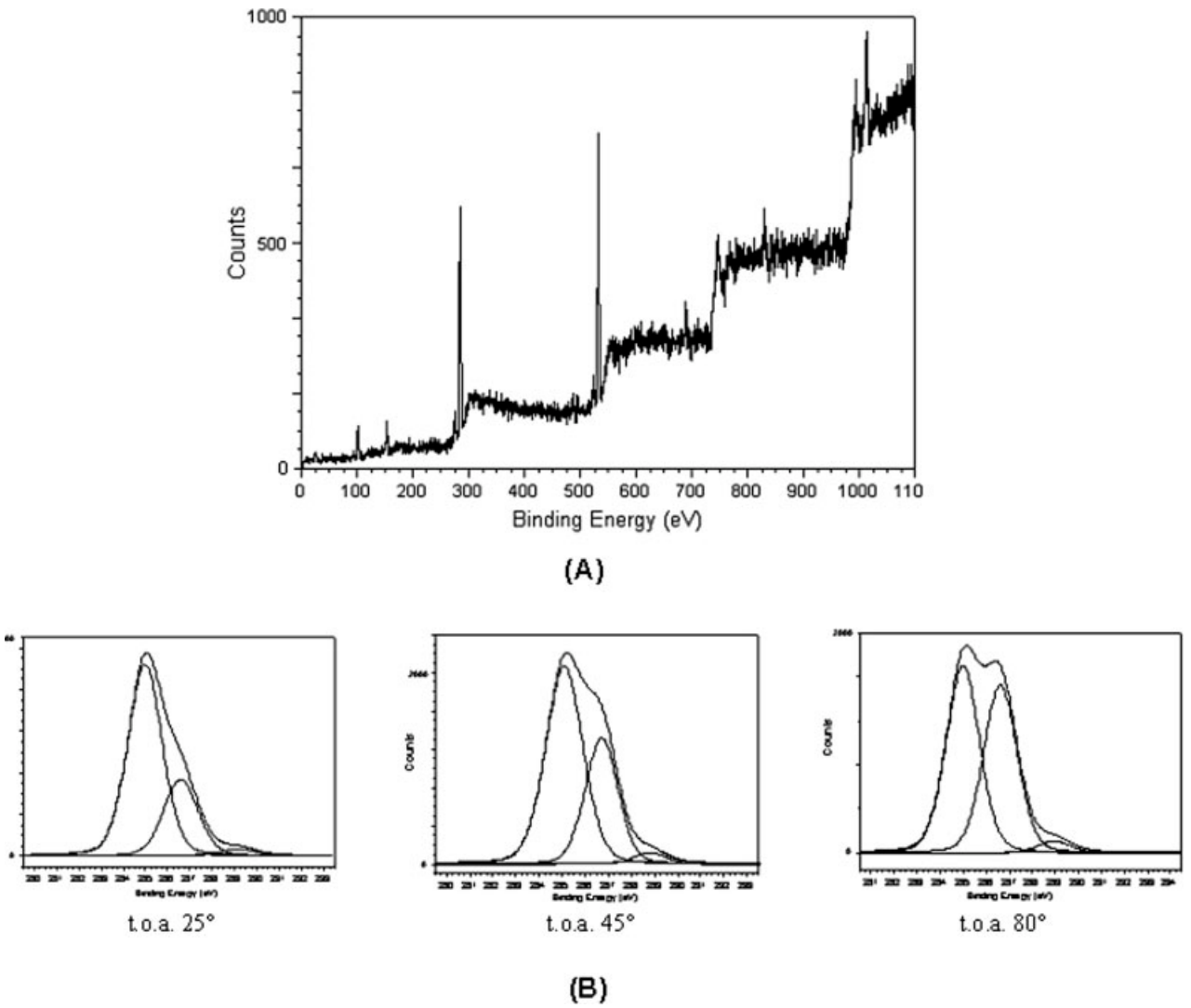

Figure 5 (A) XPS widescan spectrum at t.o.a. = 25° for hybrid film (70% w/w TEOS); (B) curve fitting of C_{1s} envelope at different toa for hybrid film (70% w/w TEOS).

TABLE IV
Contact Angle Values with *n*-Hexadecane for Cured Films

Sample		ϑ (°)
1	BEMA 1400	0
2	BEMA 1400 + 50% w/w MEMO	30
3	BEMA 1400 + 50% w/w TMOS	0
4	BEMA 1400 + 6% MEMO + 70% TMOS + condensation catalysts[a]	20
5	BEMA 1400 + 6% MEMO + 70% TEOS + condensation catalysts[a]	22

[a] Hybrid films.

After the peak fitting elaboration was done [Fig. 4(B)], the weight percentage of BEMA, MEMO, Darocur 1173, and hydrocarbon contamination were calculated through an iteration process that resulted in crossfitting the experimental atomic ratio with the obtained percentage abundance of the four components of C_{1s} envelope. The results are listed in Table II.

The data clearly indicate that MEMO shows a preferential segregation on the outermost layers of the film. These segregation phenomena can be attributed to the low polarity of the oxypropyltrimethoxysilane group present in MEMO. Similar Si enrichment was measured for systems containing polysiloxanes added to epoxy resins structures.[19]

The same aforementioned procedure was used for investigating samples obtained from BEMA + 70% (w/w) of TEOS mixtures. In Table III, the C/O and Si/O atomic ratios at different t.o.a. referred to these hybrid systems, together with the hydrocarbon contamination percentages, are collected. A typical wide-scan spectrum recorded at t.o.a. = 25° is reported in Figure 5(A) and the result of the peak fitting elaborations in Figure 5(B).

The data collected in Table III show an increase of the Si/O ratio towards the surface with respect to the bulk composition, while the corrected C/O ratio slightly decreases. Taking into account the results of Table II, the increase of the Si/O ratio and the decrease of C/O at the very surface of the films can be attributed to a selective segregation of MEMO on the surface.

Wettability measurements

The wettability properties of the cured films were investigated through contact angle measurements using *n*-hexadecane as measuring liquid. The results are collected in Table IV.

As expected, the pure UV-cured BEMA 1400 resin (sample No. 1), because of its polarity, gives rise to a contact angle value of 0°. In the presence of 50% (w/w) of MEMO (sample No. 2), the surface tension of the cured film decreases, thus the contact angle with *n*-hexadecane increases (ϑ = 30°). This value is in agreement with the XPS measurements reported in Table II, which indicate an enrichment of MEMO at the surface. The contact angle value of sample No. 2 can be attributed to the presence of cured oxypropyltrimethoxysilane groups at the surface.

The mixtures containing the same amount of TEOS (50% w/w) could not be examined, because of their inhomogeneity. Using the same mixtures containing TMOS (sample No. 3), a contact angle value of 0° was observed. These results indicate that TMOS does not change the wettability of the cured films in the adopted conditions.

The hybrid systems (sample Nos. 4 and 5) containing MEMO and TMOS or TEOS show contact angle values very close to sample No. 2, indicating the migration of MEMO at the surface, according to the XPS data (Table III).

SEM characterization and adhesion

To characterize the bulk structure of the hybrids, SEM analyses were performed on the cross-section of the films (thickness = 10 μm) coated on PET substrates. In Figure 6, a typical SEM micrograph related to the cross section of a BEMA + 70% TEOS hybrid film coated on PET is reported. The Si content, determined by EDS analysis at different depth, was found constant, moving from the PET surface towards the air–surface of the films, for all the spots investigated. Moreover, Figure 6 indicates that a regular interface between the coating and the PET film is obtained, which allows to forecast a good adhesion. The results of the adhesion measurements, performed by cross-hatching technique, confirm that in any case the adhesion is complete.

Evaluation of the barrier properties

To evaluate the barrier properties of the hybrid products, the oxygen flux through samples of PET, pure and coated with a typical hybrid coating based on

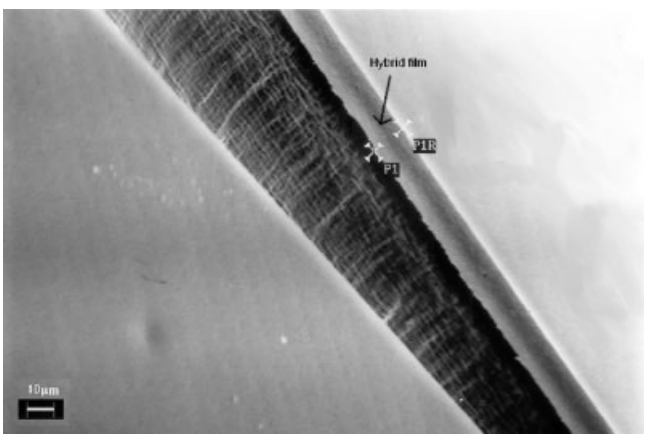

Figure 6 SEM image of a typical hybrid film (70% w/w TEOS) coated on PET.

TABLE V
Oxygen Permeability in Amorphous and Semicrystalline PET and Transport Properties at 35 and 65°C for the Systems Investigated

	OTR × 10^3 [cm^3 (STP)/(cm^2 d atm)]	Permeability × 10^2 (Barrer[a])	Diffusivity × 10^8 (cm^2/s)	Time-lag (s)
23°C[b]				
Amorphous PET ($\phi_C = 0.01$; $\rho = 1.3354$ g/cm^3)		6.47	0.6	
Semicrystalline PET ($\phi_C = 0.39$; $\rho = 1.3868$ g/cm^3)		3.05	0.3	
35°C[c]				
Amorphous PET ($\rho = 1.335$ g/cm^3)		9.77		
35°C[d]				
PET (36 μm)	7.6	4.2 ± 0.5	0.6	376
PET + BEMA (37.2 μm)	8.2 ± 0.2			371 ± 5
PET + hybrid coating (37.2 μm)	6.2			577 ± 17
Hybrid coating (1.2 μm)		0.63 ± 0.05		
65°C[d]				
PET (36 μm)	19.5	10.7 ± 0.5	2.3	95
PET + BEMA (37.2 μm)	19.1			97
PET + hybrid coating (37.2 μm)	14.1			180 ± 6
Hybrid coating (1.2 μm)		1.1±0.1		

[a] Barrer = 10^{-10} (cm^3 (STP) cm)/(cm^2 s cmHg).
[b] Ref. 16.
[c] Ref. 20.
[d] This work.

BEMA and 70% (w/w) of TEOS, was measured. Its performance was compared to pure UV-cured BEMA coated PET film without TEOS.

In Table V, the oxygen transport properties in the materials investigated, in terms of TR, time-lag, permeability, and diffusivity (only for the homogeneous materials), at 35 and 65°C are collected. The data are the average values obtained from at least two permeation experiments, and the errors represent the scattering of the experimental data. The permeability of the hybrid coating has been calculated with eq. (4): the error on P_c represents the effect of a ±0.1 μm error on the value of l_c.

The permeance of PET is reduced after addition of the hybrid coating, by a factor of 18% at 35°C and of 28% at 65°C, while the addition of pure BEMA does not determine a significant variation of the TR. The hybrid coating also allows to slow down remarkably the permeation process, as the time-lag value of the hybrid coated material is 53 and 90% higher than that of pure PET at 35 and 65°C, respectively. The pure organic coating without TEOS does not yield any significant variation of the time-lag value with respect to the pure PET sample.

As a comparison, in Table V the values of permeability and diffusivity of oxygen in pure PET at 23°C, as reported by Hu et al.,[20] and at 35°C as reported by Polyakova et al.,[21] are also listed. They refer to an amorphous sample of PET (crystallinity = 1%) and to a semi crystalline one (39%). A good agreement with the data reported in this work for both the permeability and the diffusivity values is achieved.

CONCLUSIONS

PET films were coated by hybrid organic–inorganic nanocomposites containing PEO segments linked to a methacrylate network and prepared through a dual-curing process (condensation of alkoxysilane groups subsequent to photopolymerization of methacrylic functionalities).

The surface properties of the obtained films were investigated through XPS analyses, which evidenced a selective enrichment of MEMO towards the outermost layers of the films. Contact angle measurements with *n*-hexadecane were in agreement with the XPS results.

For all the spots investigated, SEM-EDS analyses, performed on the cross-section of the hybrid films, showed a constant Si content, moving from the PET surface towards the air–surface of the films.

The hybrid materials coated on PET substrates evidenced a significant decrease of the permeability and of the OTR with respect to pure PET. These results can be attributed to the presence of silica nanophases, which determine an increase of the length of the path of the molecules through the film. They indicate the interest of such hybrid systems in packaging applications.

References

1. Yano, S.; Iwata, K.; Kurita, K. Mater Sci Eng 1998, C, 75.
2. Wen, J.; Wilkes, G. L. Chem Mater 1996, 8, 1667.
3. Tian, D.; Dubois, Ph.; Jerome, R. J Polym Sci Polym Chem 1997, 9, 2295.

4. Tian, D.; Blancher, S.; Dubois, Ph.; Jerome, R. Polymer 1998, 39, 855.
5. Messori, M.; Toselli, M.; Pilati, F.; Fabbri, E.; Fabbri, P.; Busoli, S.; Pasquali, L.; Nannarone, S. Polymer 2003, 44, 4463.
6. Mascia, L. Trends Polym Sci 1995, 3, 61.
7. Lange, J.; Wyser, Y. Packag Technol Sci 2003, 16, 149.
8. Wu, K. H.; Chang, T. C.; Wang, Y. T.; Chiu, Y. S. J Polym Sci Polym Chem 1999, 37, 2275.
9. Chang, T. C.; Wang, J. T.; Hong, J. S.; Chiu, Y. S. J Polym Sci Part A: Polym Chem 2000, 38, 1772.
10. Wei, Y.; Jin, D.; Xu, J.; Baran, G.; Qiu, K. Y. Polym Adv Technol 2001, 12, 361.
11. Zhu, Z.; Yang, Y.; Yin, J.; Qi, Z. J Appl Polym Sci 1999, 73, 2977.
12. Malucelli, G.; Priola, A.; Sangermano, M.; Amerio, E.; Zini, E.; Fabbri, E. Polymer 2005, 46, 2872.
13. Cho, J.; Ju, H.; Hong, J. J Polym Sci Part A: Polym Chem 2005, 43, 658.
14. Zou, K.; Soucek, M. D. Macromol Chem Phys 2004, 205, 2032.
15. Priola, A.; Gozzelino, G.; Ferrero, F.; Malucelli, G. Polymer 1993, 34, 3653.
16. Pizzi, D.; De Angelis, M. G.; Doghieri, F.; Giacinti Baschetti, M.; Sarti, G. C. Chemical Engineering Transactions; Pierucci, S., Ed.; AIDIC, 2005; Vol. 6, p 515.
17. Ceccorulli, G.; Zini, E.; Scandola, M. Macromol Chem Phys 2006, 207, 864.
18. Briggs, D.; Seah, M. P., Eds. Practical Surface Analysis, 2nd ed.; Wiley: New York, 1990; Vol. 1, p 437.
19. Sangermano, M.; Bongiovanni, R.; Malucelli, G.; Priola, A.; Pollicino, A.; Recca, A.; Jonsson, S. J Appl Polym Sci 2004, 93, 584.
20. Hu, Y. S.; Liu, R. Y. F.; Rogunova, M.; Schiraldi, D. A.; Nazarenko, S.; Hiltner, A.; Baer, E. J Polym Sci Part B: Polym Phys 2002, 40, 2489.
21. Polyakova, A.; Liu, R. Y. F.; Schiraldi, D. A.; Hiltner, A.; Baer, E. J Polym Sci Part B: Polym Phys 2001, 38, 1889.